Terra Antartica
2000, **7**(3), 401-412

Soft-Sediment Deformation Features in Core from CRP-2/2A, Victoria Land Basin, Antarctica

S. PASSCHIER

Department of Geological Sciences and Byrd Polar Research Center
The Ohio State University, 130 Orton Hall, 125 South Oval Mall, Columbus OH 43210 - USA (passchier.1@osu.edu)

Received 5 August 1999; *accepted in revised form* 10 December 1999

Abstract - Sediment deformation features in CRP-2/2A were described during normal logging procedures and from core-scan images. In this paper the origin of soft-sediment folding, contorted bedding, microfaulting, clastic dykes, shear zones and intraformational breccias is discussed. The features have a stratigraphic distribution related to major unconformities and sequence boundaries. Hypotheses for the origins of sediment deformation include hydrofracturing, subglacial shearing, slumping, and gas hydrate formation. Shear zones, microfaults, clastic dykes and contorted bedding within rapidly deposited sediments, suggest that slumping in an ice-distal environment occurred in the early Oligocene. A till wedge beneath a diamictite at 364 mbsf in the mid-Oligocene section represents the oldest evidence of grounded ice in CRP-2/2A. Shear zones with a subglacial origin in the early late Oligocene and early Miocene sections of the core are evidence of further grounding events. The interpretation of sediment deformation in CRP-2/2A is compared to other Antarctic stratigraphic records and global eustatic change between the late Eocene/early Oligocene and the middle Miocene.

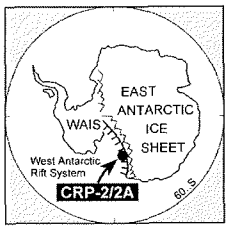

INTRODUCTION

The Cape Roberts Project aims at reconstructing the Cenozoic climatic and tectonic history of the Transantarctic Mountains and the East Antarctic craton. The Cape Roberts CRP-2 and 2A holes are located ca. 15 km east of Cape Roberts (Fig.1). CRP-2 terminated at 57 metres below the sea floor (mbsf) and a new hole, CRP-2A, was started at the same site. Drilling took place in a water depth of 178 m with a core recovery of more than 91 % for CRP-2 and 95 % for CRP-2A. The composite record of CRP-2 and 2A (referred to as CRP-2/2A) comprises an early Oligocene to Quaternary section down to 624 mbsf. The drillholes are located on the north-south trending Roberts Ridge, which forms the western margin of the Victoria Land Basin, a 20 km wide rift depression (Hamilton et al., 1998). The Transantarctic Mountains form the rift flank, which is separated from the basin by a major fault at ca. 10 km west of the drillsites. Drilling takes place in a sedimentary wedge extending from the Transantarctic Mountains. The sedimentary wedge is now truncated to the north by the glacially eroded Mackay Sea Valley, reaching water depths of over 1000 m. Microfossils suggest a predominantly shallow marine setting for the cored interval, although some core intervals are barren (Cape Roberts Science Team, 1999). Repetitive facies associations of diamictites, sandstones and siltstones, are indications of cyclical changes in glacial proximity and water depth. A 150 metre thick late Oligocene section bracketed by Ar/Ar dates on volcanic ash spans only *ca.* 300 000 yrs, suggesting that much of the record is missing at unconformities.

This paper deals with structures, which developed in the early burial history of the sediment. Therefore, these structures can be related to the depositional and erosional processes, which were responsible for the accumulation and reworking of semi- or unconsolidated sediment.

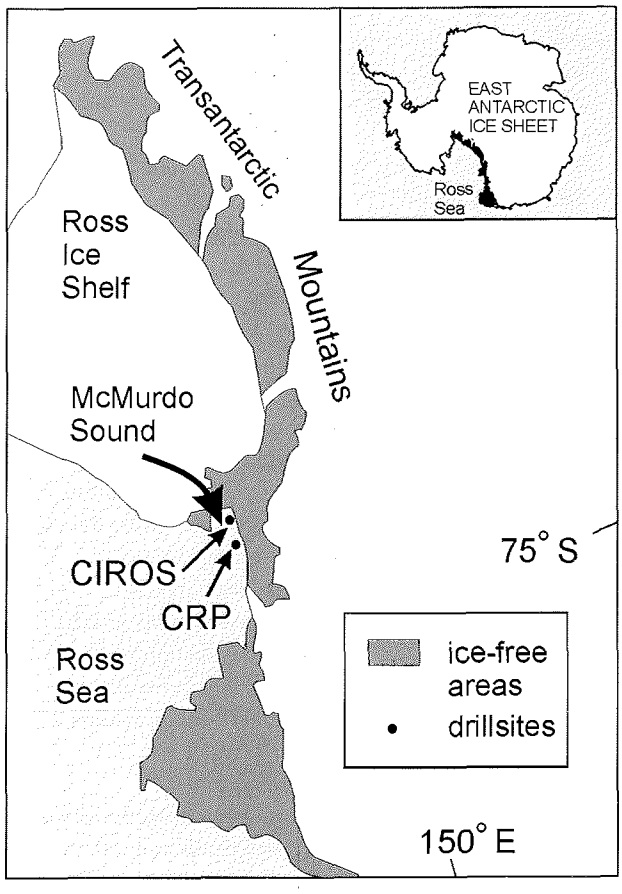

Fig. 1 - Map of the Ross Sea area, showing the location of the CRP drillsites, the CIROS-1 drillsite and the ice-free Transantarctic Mountains.

Sediment deformation features were recorded on the cut surface of the CRP-2/2A cores during normal logging procedures and on core-scan images after drilling was completed. Two whole-core thin sections from CRP-1 were also examined. CRP-1 penetrated an interval of similar age to the upper part of CRP-2/2A and was drilled *ca.* 1 km to the east of CRP-2/2A (Cape Roberts Science Team, 1998). Coring induced deformation was recognised, which was partly a result of pre-existing natural fractures in the sediment. Many deformation features occur in now consolidated core, including healed fractured sediment, here called breccia.

Tab. 1 - List of prominent deformation features and interpretation in CRP-2/2A.

Deformed interval (mbsf)	Deformation type	Facies association	Interpretation
12-16	crackle breccia?	bottom of diamictite	?
44.91-47.87	chaotic breccias, thrusts	above diamictite	proglacial ice-push
50-71	breccias, cataclastic shear zones	below diamictite	subglacial shear
90.67-92.86	soft-sediment deformation	below diamictite	subglacial shear?
93.85-98.64	crackle breccia	between diamictites	*in situ* fracturing
99	folding	within diamictite	mass-gravity flow
131-132	crackle breccia	below diamictite	*in situ* fracturing
145-151	brecciated sandstone dykes	top of clast-poor unit	hydrofracturing
176.2-176.3	microfaults, soft-sediment folding	within mudstone	?
183.35-185.95	folds, rotated clasts	top of sandstone	mass-gravity flow
245	vertical fractures	below diamictite	?
297.4	clastic dyke through cemented patch	above diamictite	?
297-306	folds (D), faults and breccia (sst)	within diamictite	collapse?
306	intraclast, boudinage, clast rotation	bottom of diamictite	subglacial shear
307	fault with large displacement	below diamictite	?
307-308	rubble and crackle breccia	below diamictite	subglacial shear
311-315	matrix-supported breccia	within clast-poor unit	collapse?
315-326	faults and clastic dykes	interbedded lithologies	?
328	clastic dyke, coarse stratified fill	below diamictite	subglacial shear
329	clastic dyke?	below diamictite	subglacial shear
331.9	matrix-supported breccia	within mudstone	mass-gravity flow
332	clastic dyke, calcified and pyritized	within mudstone	?
334	clastic dyke, faulted	within mudstone	?
337	clastic dyke, folded and faulted	within mudstone	?
362.78-363.08	shear zone, folding, faulting	between diamictites	subglacial shear
363.22-363.63	clastic wedge	between diamictites	subglacial shear
364	clastic dyke	between diamictites	subglacial shear
381-384	microfaults, soft sediment folding	stratified diamictite	mass-gravity flow
447	pyritised clastic dikes, planar margins	within mudstone	tectonic?
468.7	fault cross-cuts calcite patch	within mudstone	tectonic?
501-503	contorted bedding, folding	laminated sandstone	slumping
504-506	local mosaic breccias	interbedded lithologies	gas-hydrate formation?
512-516	contorted bedding, folding	graded beds	slumping
520-523	clastic dykes, microfaulting	sandy conglomerate	debris flow
524-527	faults, pyritised clastic dykes	below congomerate	debris flow
525.8	mosaic breccia	above graded beds	gas-hydrate formation?
535-540	faulted clastic dykes	below congomerate	debris flow
543-552	faults, pyritised clastic dykes	within mudstone	tectonic?
577-579	contorted bedding, folding	interbedded lithologies	slumping
579.02-580.99	anastomosing networks	interbedded lithologies	slumping
581-585	contorted bedding, folding	above conglomerate	slumping
587	mosaic breccia	above graded beds	gas-hydrate formation?
594.97-595.03	mosaic breccia	below clast	gas-hydrate formation?
608.7	anastomosing dilated laminae	below stratified sandst	slumping
608-614	contorted bedding, folding	within sandstone	slumping
612.00-612.07	microfaulting cuts folding	above conglomerate	slumping
614.0-614.2	anastomosing dilated laminae	above conglomerate	slumping

Sedimentation rate and glacial proximity are the primary controls on the stability of the depositional environment. Lithofacies and sequence stratigraphic interpretations suggest that the grounding line of glaciers repeatedly approached and abandoned the location of the drillsite (Cape Roberts Science Team, 1999). Since the reconstruction of Antarctic ice-volume is a main objective of the project, macroscopic (this study) and microscopic analyses (Van der Meer, this volume) of sediment deformation features are performed to identify subglacial overriding. Sheared breccias were already linked to glacial overriding in the Miocene section of CRP-1 (Passchier et al., 1998). Other deformation features encountered in the CRP-2/2A core, such as contorted bedding with preserved lamination, clastic dykes and microfaults, also help to characterise ice-distal depositional environments.

CHARACTERIZATION OF THE DEFORMATION

Both "ductile" and "brittle" deformation was recorded, with the words "ductile" and "brittle" used in the following sense: "ductile" deformation as continuous flow due to grain-boundary sliding and Mohr-Coulomb failure of unlithified overpressurised sediment; "brittle" deformation as grain-boundary sliding of dewatered sediment showing dislocation of sedimentary fabric along discrete planes. Main features observed are: intraformational brecciation, clastic dykes, folding, contorted bedding, reverse and normal microfaulting, shear zones and slip planes. Detailed descriptions of some features can be found in the CRP-2/2A Initial Report (Cape Roberts Science Team, 1999) and the most prominent features are listed in table 1.

Brecciation in CRP-2/2A is similar to the patterns described in Passchier et al. (1998) from CRP-1. The breccias consist of fractured sediment or intraformational sediment clasts in a matrix. Five types of breccias occur in CRP-2/2A: 1) crackle breccias and 2) mosaic breccias (Fig. 2), which are defined as *in situ* fractured rock; 3) rubble breccias, which consist of rounded pebbles; 4) chaotic breccias, with large fractured clasts within a matrix; and 5) matrix-supported breccias. Similar to CRP-1 breccia fabrics occur in stacked patterns of *in situ* brecciated intervals grading into rubbly and chaotic zones. Some unconsolidated brecciated sandstones in the upper part of the CRP-2/2A core (~45-48 mbsf) have a thrusted fabric (Fig. 2c). An extremely thick mudstone breccia is found between 311 and 315 mbsf in CRP-2/2A. The breccia has angular clasts, which are tightly packed in a sandstone matrix. Similar lithologies as the mudstone clasts are preserved beneath the breccia.

Three kinds of clastic dykes can be recognised in CRP-2/2A: 1) dykes with irregular boundaries and coarse infill, with various orientations from near horizontal to vertical; 2) near-vertical dykes with an apparent homogeneous infill and planar boundaries; and 3) homogenous clastic injections accompanied by brecciated host rock (Fig. 3). Thin sections were available from two dykes with planar margins in the early Miocene section of CRP-1 (Fig. 4). Similar clastic dykes occur in the Oligocene section of

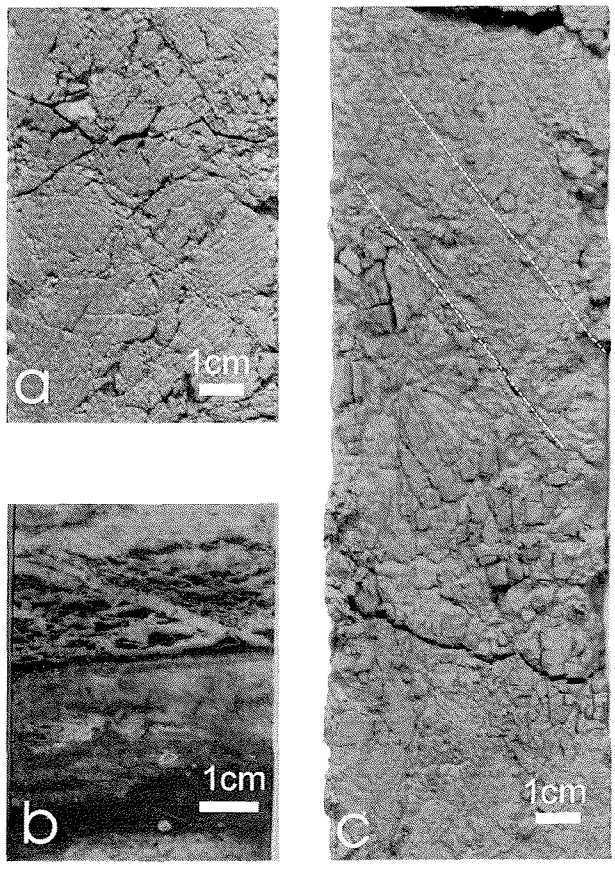

Fig. 2 - Breccias from CRP-2/2A: a) crackle breccia at ca. 56 mbsf; b) mosaic breccia at ca. 505 mbsf; and c) deformed breccia at ca. 45 mbsf. Note the thrusted fabric in (c).

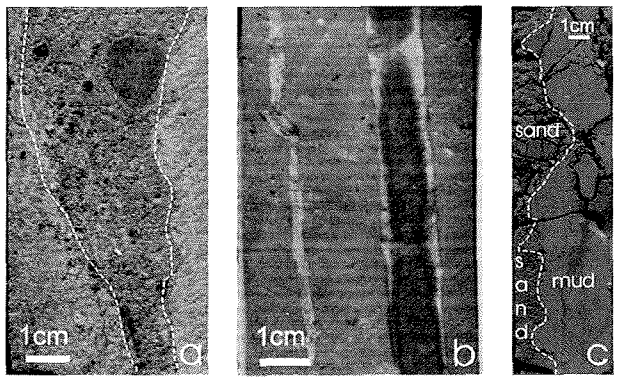

Fig. 3 - Clastic dykes from CRP-2/2A: a) wedge-shaped dyke with irregular margins, filled with poorly-sorted sandstone at 363 mbsf; b) pyrite and carbonate cemented sandstone dyke with planar margins at 446 mbsf; c) brecciated medium sandstone dyke at 145 mbsf. The fabric of the brecciated mudstone (c) suggests injection occurred from below.

CRP-2/2A, but these dykes are cemented by pyrite in the centre and by calcite along the walls. A clastic dyke crosscuts a calcite-cemented patch at 297.4 mbsf in CRP-2/2A.

Microfaults comprise both reverse and normal faults, normal faults being more abundant (Fig. 5). The microfaults occur both as single slip planes and as sets of parallel fault planes. Some faults are bounded by folded strata, (*e.g.* ~612 mbsf) or display drag along the fault plane. Faults in the lower Oligocene part of the section are frequently mineralised (Fig. 5c). A fault crosscuts a calcite-cemented patch at 468.7 mbsf in CRP-2/2A. Some normal faults were injected by sediment in a later stage and are classified as clastic dykes.

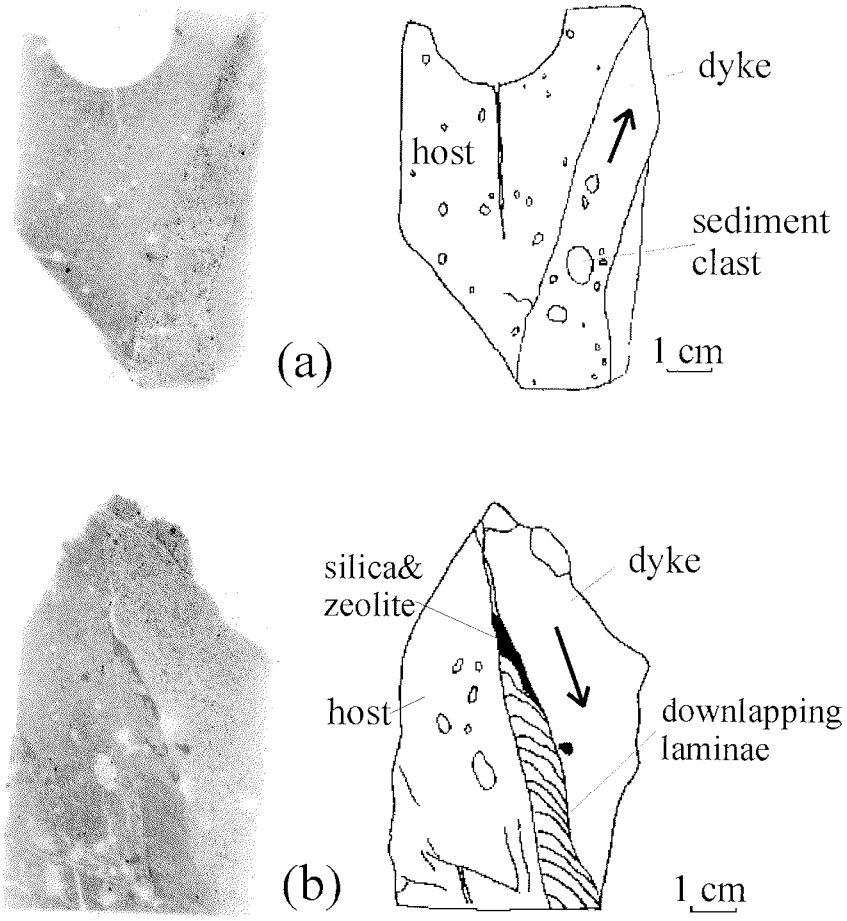

Fig. 4 - Clastic dykes from CRP-1: a) thin section (left) and interpretation (right) of clastic dyke at 133 mbsf; and b) thin section (left) and interpretation (right) of clastic dyke at 133 mbsf. The dykes are filled with concentrically-zoned carbonate microconcretions of the types encountered in fractures in other parts of the core (Baker & Fielding, 1998). Microconcretions in sediments of the upper dyke are smaller than those in the lower dyke. The presence of a diamictite intraclast with small microconcretions in the upper dyke (a) suggests that the pebble was derived from a lower level in the stratigraphic column. Downlapping laminae in the lower dyke suggest settling of sediment occurred as water pressures diminished. However, the downlapping laminae are truncated, suggesting that the dyke was reactivated after deposition of the laminae. Rapid fluctuations in water pressures in dyke systems are characteristic of subglacial and proglacial environments (Van der Meer et al., 1994, Von Brunn & Talbot, 1986).

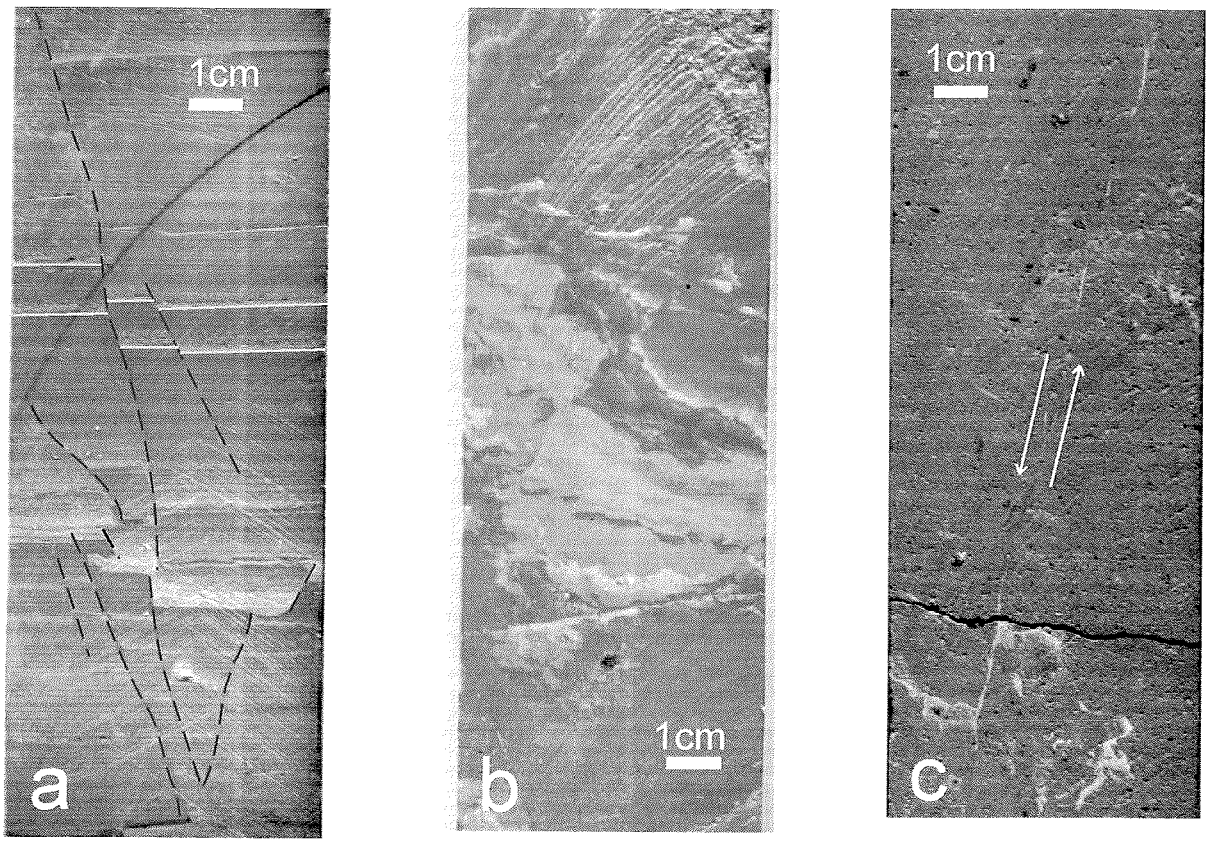

Fig. 5 - Microfaults from CRP-2/2A: a) micro-block faulting in laminated sediments at 319 mbsf; b) reverse microfaulting in subglacially deformed sediments at 363 mbsf; c) normal microfaulting with carbonate cemented fault plane at 543 mbsf. Faults a) and c) are compatible with an extensional stress regime, however do not necessarily share the same origin. Fault b) may have formed in a compressional stress-regime associated with glacial overriding.

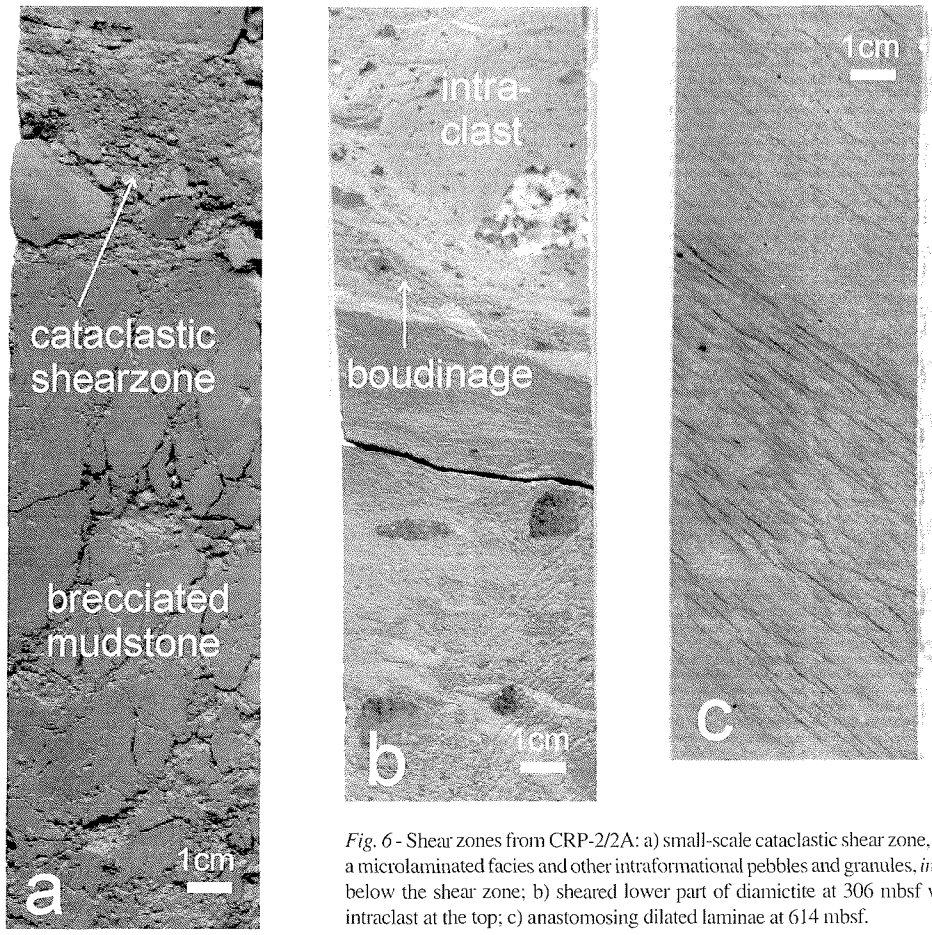

Fig. 6 - Shear zones from CRP-2/2A: a) small-scale cataclastic shear zone, with an intraclast of a microlaminated facies and other intraformational pebbles and granules, *in situ* crackle breccia below the shear zone; b) sheared lower part of diamictite at 306 mbsf with boudinage and intraclast at the top; c) anastomosing dilated laminae at 614 mbsf.

Shear zones and slip planes can be classified as 1) small-scale cataclastic shear zones (Fig. 6a); 2) soft-sediment folding progressing into bedding attenuation (Fig. 6b); and 3) anastomosing, augen-like, dilated laminae (Fig. 6c). The cataclastic shear zones occur in association with breccias and consist of intraformational abraded pebbles and granules within cemented fine sandstones. The second type of shear zone is sometimes associated with boudinage, diamictite intraclasts, and rotated clasts with pressure shadows. The anastomosing, augen-like dilated laminae form shear bands up to > 1 m thick.

Contorted bedding is identified in intervals of core with interstratified fine sandstone and siltstone (Fig. 7). Axial planes of folds are oriented in all directions including horizontal. The chaotic folding of sediment is associated with dipping strata (15-20 degrees) and shear zones of the anastomosing network type.

STRATIGRAPHIC DISTRIBUTION OF SEDIMENT DEFORMATION FEATURES

Intense deformation is confined to three intervals in CRP-2/2A (Fig. 8). The character of the deformation changes downcore (Tab. 1). The uppermost deformed interval is characterised by brecciation, small-scale cataclastic shear zones and minor soft-sediment deformation. Localised *in situ* brecciation first occurs in the CRP-2/2A core at 12 mbsf, in a Quaternary diamicton. Brecciation intensifies at 38 mbsf

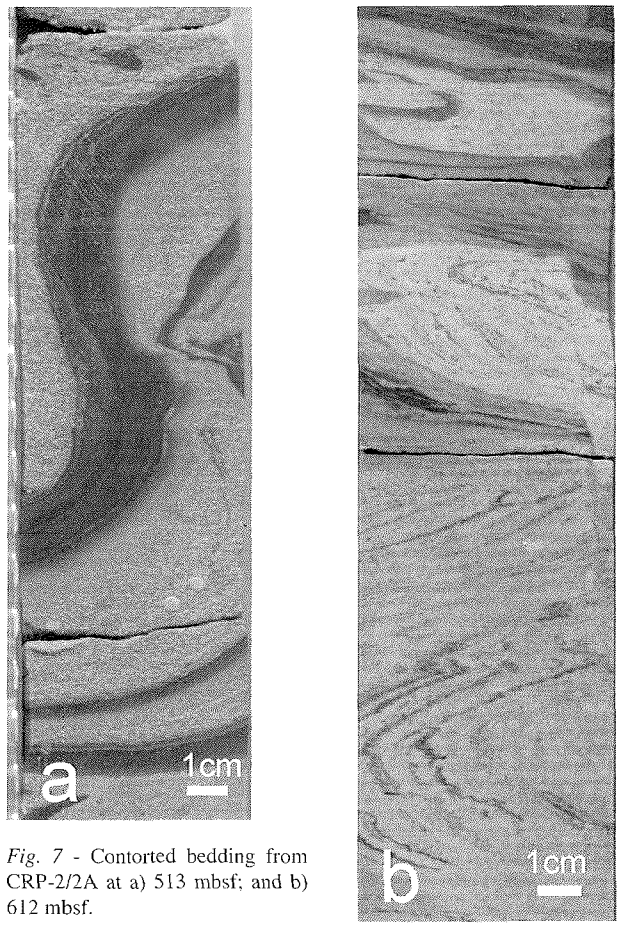

Fig. 7 - Contorted bedding from CRP-2/2A at a) 513 mbsf; and b) 612 mbsf.

and decreases below 151 mbsf, ca. 20 m below the Miocene-Oligocene boundary (*ca.* 130 mbsf). A relatively undeformed interval is present between 151 and 297 mbsf in the uppermost Oligocene section of the core.

Deformation intensifies at *ca.* 297 mbsf. Faults, clastic dykes and shear zones dominate in the interval between 297 and 401 mbsf. At 306 mbsf the bottom of a diamict contains a diamict intraclast, overlying boudinaged mudstone and breccia (Fig. 6b). A thick matrix-supported mudstone breccia occurs at 311-315 mbsf. A shear zone and a clastic wedge occur below a diamictite at 362-364 mbsf. Faulted dykes occur at 334, 337 and 535-540 mbsf.

The character of the deformation changes markedly below 485 mbsf. The sediments in this interval of core are now strongly lithified, but display deformation caused in an unlithified, perhaps sometimes water-saturated condition, illustrated by clastic dykes with irregular flow margins (*e.g.* 517.6 mbsf). Contorted bedding is recognised at 501-503, 512-516, 577-579, 581-585 and 608-614 mbsf. Thin mosaic breccias also occur below *ca.* 500 mbsf (Fig. 2b). Anastomosing (augen-like) dilated shear zones are present at 580, 608 and 614 mbsf. Bedding is inclined > 15 degrees below 606 mbsf.

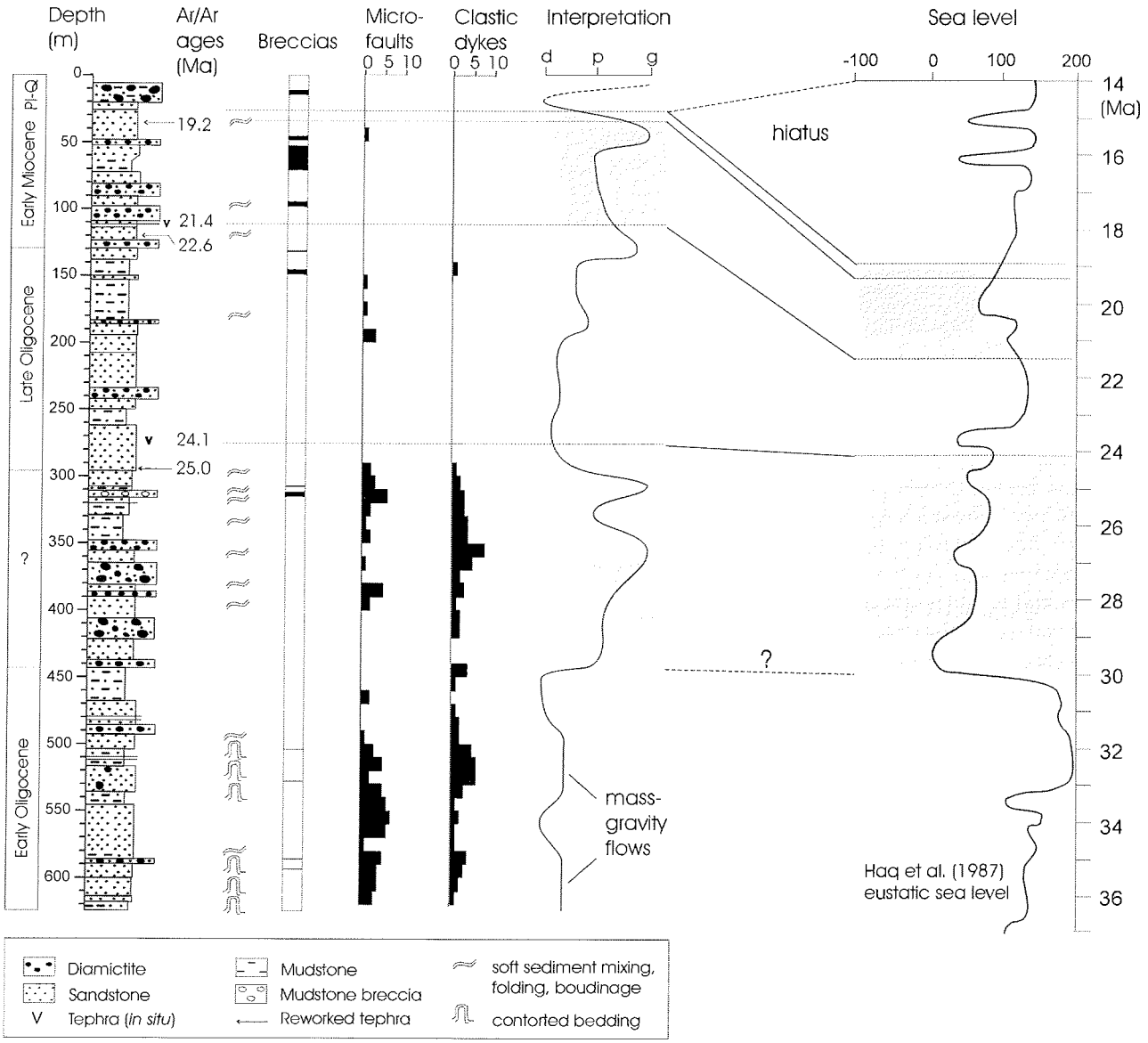

Fig. 8 - Downcore distribution of ductile and brittle sediment deformation features. Clastic dykes and microfaults are recorded as the number of features per 10 m intervals of core. In the interpretation column d, p, and g refer to the proximity of the grounding line with respect to the drillsite: d=distal, p=proximal, g=grounded. Lithological column and chronology from Cape Roberts Science Team (1999). Ar/Ar ages are from McIntosh (this volume). Eustatic curve from Haq et al. (1987). Mass-gravity flows in the early Oligocene correspond to sea level highstands of the Haq et al (1987) eustatic curve. The mid-Oligocene lowstand corresponds to the initiation of abundant diamictite deposition culminating into grounding of ice on the drillsite. The uppermost Oligocene section does not show any evidence of grounded ice near the drillsite, but a sea level lowstand does occur. A highstand characterises the early Miocene, but grounded ice occasionally reached the drillsite.

DISCUSSION

ORIGIN OF THE DEFORMATION

On glaciated continental margins both glacial and marine processes affect deposition, erosion, and deformation of sediment. At present the Cape Roberts drillsite is characterised as a polar interglacial depositional environment. Other cores from McMurdo Sound and seismic interpretations suggest that ice grounded on the shelf periodically since at least the Oligocene (Bartek et al., 1996). However, whether a thick continental ice-sheet grounded on the shelf or local outlet glaciers is unknown.

Glaciers or ice-sheets terminating on continental margins overly unlithified sediment beds. Subglacial shear deformation occurs when subglacial drainage is poor, resulting in high pore-water pressures at the ice-bed interface. Subglacial shear deformation results in remoulding of sediments into what is called a deformation till or a deforming bed. Deforming beds have been found underneath many modern glaciers and ice-sheets (Boulton & Hindmarsh, 1987; Murray, 1997; Alley et al., 1997) and the characteristic features of subglacial shear deformation have been well-documented from outcrop studies of Pleistocene and Recent glacial deposits (Croot, 1988; van der Wateren, 1995). In a marine environment, the typical stratigraphic position for the presence of glaciotectonic features is at the bottom of, or below diamictites, which are deposited during the retreat stage in subglacial and proglacial environments near the grounding line. Deformation found within the upper part of diamicts or in overlying sediments may originate from slumping (Dreimanis, 1993).

Shear zones

Shear zones at 306 and 363 mbsf occur at the bottom of diamictites and are likely caused by glacial overriding (Fig. 6b). The features are similar to those described from shear zones below soft-bedded Pleistocene ice-sheets (Van der Wateren, 1995, p. 75).

Cataclastic shear zones, such as occur at ca. 67 mbsf in CRP-2/2A (Fig. 6a), are not described from Pleistocene Northern Hemisphere glacial deposits, but were also encountered in CRP-1 (Passchier et al., 1998). Deformation of basal sediment at sub-freezing temperatures occurs along well-defined shear planes, demonstrating more brittle failure characteristics of the basal layer (Echelmeyer and Wang, 1987). However, in CRP-1 the sheared breccias show evidence of fluidised sediment remobilization (Passchier et al., 1998), suggesting that basal conditions were, at least periodically, above the pressure melting point. The cataclastic shear zones are confined to the Miocene sections of the CRP-cores and may represent polythermal basal conditions, intermediate between the margins of Pleistocene temperate ice-sheets and sub-freezing basal conditions. Lower subglacial pore-water pressures result in a more brittle style of deformation as represented by the sheared breccias (Brodzikowksi & Van Loon, 1985). The absence of great numbers of clastic dykes and microfaults in the early Miocene section may also indicate more stable proglacial environments, suggesting lower meltwater production rates and reduced proglacial sedimentation rates.

Anastomosing network shear zones are confined to the lower part of the core (Tab. 1). No association with glacial facies exists. The great thickness of some of the shear zones suggests that displacement of large masses of sediment occurred. The augen-like shear zones may represent the basal slide planes of slumps, a rotational form of slope failure (Martinsen, 1994). This interpretation is supported by the presence of inclined beds in the lower part of the core.

Breccias

Cataclastic shear zones cut through *in situ* fractured sediment in CRP-2/2A (Fig. 6a), suggesting that the fracturing preceded horizontal shearing. This in itself demonstrates that the fracturing of sediment is due to a geological process, since horizontal shearing after fracturing is not compatible with stresses induced by drilling. In addition, the cataclastic shear zones and parts of fractured core are recemented. The unconsolidated nature of the core material in the Quaternary section, makes it difficult to describe the fabrics and to identify drilling induced deformation. Therefore, the Quaternary breccias will not be further discussed here. Three mechanisms act to produce the breccia fabrics: 1) *in situ* fracturing of the semi-consolidated sediment; 2) horizontal shearing of fractured sediment producing rubble and chaotic breccias by shear-related cataclasis; 3) abrasion and transport of fractured sediment producing matrix-supported breccias with rounded clasts. Microscopic thin section observations of brecciated sediments (Van der Meer, this volume) are being performed to evaluate the mechanisms proposed here.

The presence of a sandstone dyke within a brecciated mudstone at 145-151 mbsf in CRP-2/2A (Fig. 3c) suggests a role of overpressurized, fluidised sediment in fracturing for some of the breccias. The mudstone was injected by sand from below, based on the breccia fabric and the presence of well-sorted unconsolidated sandstone below the brecciated mudstone. Hydrofracturing is a process observed and predicted in ice-marginal areas, where aquicludes overly permeable sediments (Boulton & Caban, 1995, Rijsdijk et al., 1999). Hydrofracturing may occur both subglacially and proglacially (Fig. 9b) and in both marine and terrestrial environments (Rijsdijk et al., 1999; Boulton & Caban; 1995, Dionne & Shilts, 1974; Dreimanis & Rappol, 1997; Larsen & Mangerud, 1992; Von Brunn & Talbot, 1986.) Due to the high pressures and discontinuous nature of the sediment bodies in ice-contact environments, deformation related to hydrological processes may be quite extensive beneath soft-bedded ice-sheets (*cf.* Rijsdijk et al., 1999).

Early Miocene sheared breccias below diamictites in CRP-1 were also attributed to grounded ice (Passchier et al., 1998). Carbonate cement with low $\delta^{18}O$ values in open fractures of brecciated rock in the Miocene section of CRP-1 (Baker & Fielding, 1998) may have precipitated from meteoric water. Clastic veins within sheared breccias

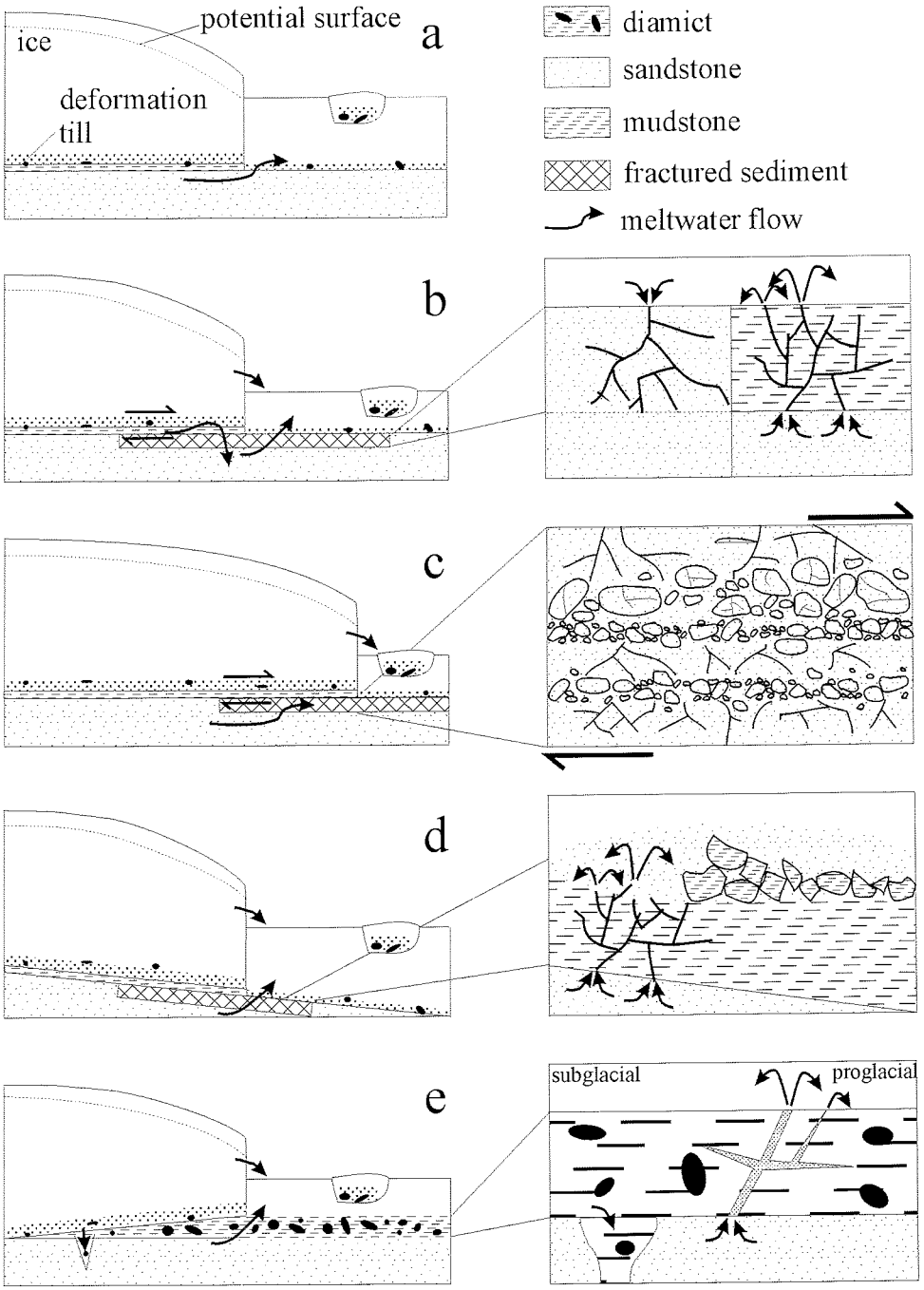

Fig. 9 - Hypotheses for the formation of meltwater-related glaciotectonic structures described from the Cape Roberts drillcores (partly after Boulton and Caban, 1995, Rijsdijk et al., 1999). (a) Free flow of meltwater, no deformation. (b) Hydrofracturing of subglacial and proglacial sand and silt. Subglacial sediment mobilisation may also occur into existing tensile fractures, formed due to ice loading. In the proglacial area low permeability of proglacial sediments or the presence of permafrost may impede free drainage when water depths are shallow. (c) Subglacial deformation of fractured sediments and cataclastic shearing. (d) Proglacial hydrofracturing and redeposition of mudstone breccia. (e) Subglacial and proglacial hydrofracturing in relation to diamictites. The high tensile strength of diamicites apparently leads to the formation of thicker clastic dykes rather than small hairline fractures as observed in sand and mud (b and d).

of CRP-1 (Passchier et al., 1998) suggested hydrofracturing occurred in a subglacial environment. However, fluidised sediment may also have been remobilized into existing tensile fractures, formed due to ice loading (Fig. 9b). Sheared breccias in the early Miocene section of CRP-2/2A probably also formed subglacially (Fig. 6a and 9c). Breccias at 45-48 mbsf in CRP-2/2A show an atypical thrusted fabric, which was not recognised in CRP-1. High angle thrusts are characteristic of proglacial ice-push environments (Van der Wateren, 1995, p. 110). The stratigraphic position of the thrusts is in accord with this interpretation (Tab. 1). The thrusted breccia immediately overlies a subglacially deformed interval and a diamictite unit.

Thin matrix-supported breccias in CRP-1 were regarded as redeposited (Passchier et al., 1998). A similar origin could be proposed for the matrix-supported mudstone

breccia at 311-315 mbsf in CRP-2/2A. However, the uniform composition and the presence of angular mudstone clasts, suggest only minor transport occurred. Perhaps the breccia represents a collapsed horizon, because all strata in the interval between 297 and 327 mbsf are deformed and normal and reverse faults are abundant. Both normal and reverse faulting in non-cohesive sands have been found in model studies of depleting reservoirs (Odonne et al., 1998). A significant unconformity must be present between 297 and 306 mbsf, based on sharp terminations in a number of datasets from the core, including sediment deformation (Cape Roberts Science Team, 1999). Evidence of glacial overriding is present at 306 mbsf, which means that a relation between brecciation and glacial proximity is likely.

Intraformational breccias are also described from the Miocene sections of the CIROS-1 (Hambrey et al., 1989a) and MSSTS-1 (Barrett & McKelvey, 1986) cores in McMurdo Sound. The coincidence of brecciated intervals in the late Oligocene-early Miocene section of CRP-2/2A and CIROS-1 is striking (Fig. 10). The Oligocene breccias in CRP-2/2A consist of a fractured mudstone injected by sand (Fig. 3c), and the thick mudstone breccia (311-315 mbsf) described above. The breccias in CIROS-1 mainly consist of mudstone clasts in a sandy mud matrix. Both Hambrey et al. (1989a) and Fielding et al. (1997) suggested that the breccias in CIROS-1 were redeposited. The cause of the initial fracturing of the sediment may be hydrofracturing as illustrated by the brecciated dyke in CRP-2/2A. Although the brecciated dyke is found *ca.* 20 m below the Oligocene-Miocene boundary, the event may have occurred during the early Miocene. An early Miocene mudstone breccia is present at a depth between *ca.* 48 and 64 mbsf below a diamictite in CIROS-1. A possible relation to a nearby grounding line cannot be ruled out, due to the presence of diamictites stratigraphically above the breccias (Fig. 9d).

Some breccias cannot be related to ice-contact glacial environments, such as the mosaic breccias, which occur below ca. 500 mbsf (Fig. 2b). The breccias occur in an interval of core with low marine productivity and slope instability inferred from sedimentary facies (Cape Roberts Science Team, 1999). The presence of an oily overprint on the sediments below *ca.* 500 mbsf may suggest organic contents are increasing downhole. Bohrmann et al. (1998, p. 649) describe brecciation as a result of the growth of gas hydrates and subsequent fracturing from Hydrate Ridge on the western North American continental margin. Gas-hydrates are solid compounds built out of water and gas (*e.g.* methane), which are stable under restricted temperature and pressure conditions (Kvenvolden, 1993). In polar regions gas-hydrates occur within shelves and permafrost areas at depths > 150 m. Dissociation of gas hydrates may cause catastrophic failure of thick sedimentary sequences (Paull et al., 1996; Maslin et al., 1998). The mosaic breccias, indications of mass-gravity flow, and the increasing organic content of the lower part of CRP-2/2A may be connected with the formation and dissociation of gas hydrate. Bohrmann et al. (1998) describe the formation of carbonate with a distinct chemical and isotopic composition in relation to hydrate development. Chemical analysis of carbonate cemented breccias in CRP-2/2A could reveal whether their formation is related to gas hydrates.

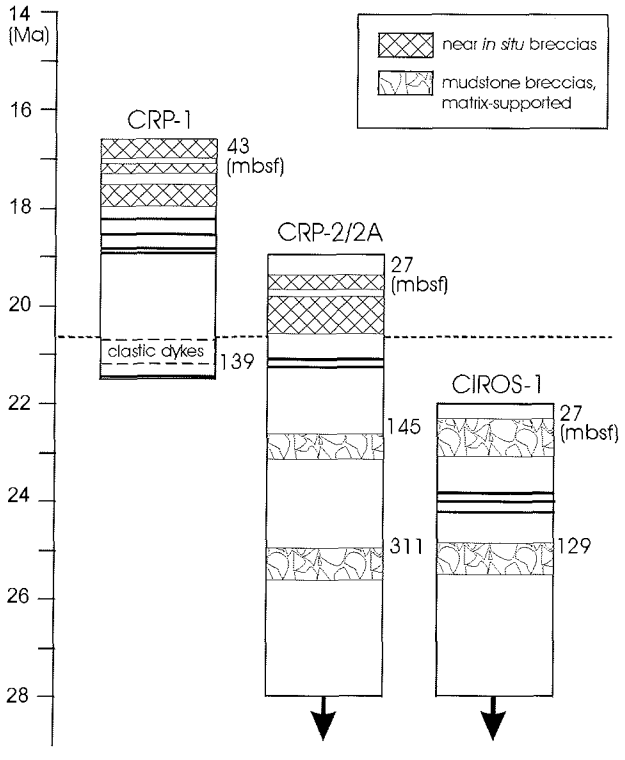

Fig. 10 - Simplified stratigraphic distribution of breccias in the Oligocene-Miocene sections of McMurdo Sound cores. Note that near *in situ* breccias predominate in the late early Miocene, whereas mudstone breccias are more abundant in the earliest Miocene to Oligocene. CRP-1 data are from Passchier et al. (1998), CIROS-1 data are from Hambrey et al. (1989a) and Fielding et al. (1997).

Clastic dykes

Clastic dykes are described from a range of environments including mass-flow (Shanmugam et al., 1996), tectonic (*e.g.* Bergman, 1982, Winslow, 1983) and glaciotectonic settings (*e.g.* Dionne & Shilts, 1974; Dreimanis & Rappol, 1997; Larsen & Mangerud, 1992; Von Brunn & Talbot, 1986). A preliminary study on two clastic dykes in an early Miocene diamictite from CRP-1 show a pattern of fluid and sediment flow (Fig. 4) consistent with formation in an ice-marginal environment. In a glacial environment clastic dykes form perpendicular to the direction of ice-flow (Fig. 9e) and can be injected upward, downward or sideways (Van der Meer et al., 1994; Dreimanis & Rappol, 1997). Wedge-shaped dykes with a diamict infill, such as at 363 mbsf in CRP-2/2A (Fig. 3a), can be interpreted as injection of till from the base of a glacier into unconsolidated sediment during glacial overriding (Dionne & Shilts, 1974). Clastic dykes from the lower part of the core (below ca. 470 mbsf) are not related to diamictites. Some of these dykes have irregular flow margins, suggesting injection occurred into fluidised sediments, compatible with formation in mass-movement environments. The fabrics of most dykes with planar margins in the lower part of the core (Fig. 3b) have been obliterated by post-depositional mineralisation. Some

dykes represent injection of sediment into mineralised normal faults. A tectonic origin for these dykes cannot be ruled out, but a glacial origin is unlikely considering the general geological context of the features.

Microfaults

The record of microfaults may include brittle features associated with the present tectonic regime of the basin (cf. Wilson & Paulsen, this volume). Macroscopically, post-lithification micro-faulting cannot be distinguished from syn-sedimentary deformation. However, the uneven stratigraphic distribution of microfaults suggests that the present tectonic stress regime is not a major cause of microfaulting throughout the section. Even microfaults and clastic dykes cross-cutting calcite cement at 297.4 and 468.7 mbsf, may have been formed due to syn-sedimentary deformation, since carbonate cementation may occur close to the sea floor. Other faults have been mineralised (Fig. 5c), suggesting development under higher temperature and pressure conditions than exist near the surface. This is particularly true for microfaults below 444 mbsf. However, most microfaults above 444 mbsf reflect a contemporaneous extensional stress regime, which is compatible with subglacial overriding and slope failure (Martinsen, 1994; Van der Wateren, 1995). Microfaulting of clastic dykes at 334, 337 and 535-540 mbsf suggests that more than one episode of deformation affected the sediments. However, both in glacial and mass-movement environments overprinting of structures is observed when deformation continues (Martinsen, 1994; Van der Wateren, 1995).

Contorted bedding

Contorted bedding is an indicator of low-strain deformation of water-saturated stratified sediments and is commonly associated with slumping in a marine environment (Shanmugam et al, 1995; Hampton et al., 1996). Inclined bedding (15-20 degrees) below 606 mbsf suggests a rotational form of slope failure, compatible with slumping. The facies association of interbedded sand- and mudstones with loading structures, and structureless sands, also suggests that slumping, debris flows and grain flows characterise the early Oligocene section of CRP-2/2A and that sedimentation rates were high. Clastic dykes with irregular margins below 485 mbsf in the CRP-2/2A core are associated with high pore-water pressures in the sediment as is common in rapidly deposited sequences. Similar to other nearby paleofjords, it is possible that the Mackay valley was a fjord during non-glacial times and that part of the record off Cape Roberts represents deposition of a fjord mouth delta. Rapid deposition on delta fronts at the mouth of fjords results in accumulation of underconsolidated sediments with high pore-water volumes, and therefore low shear strength (Syvitski et al., 1987). The seismic interpretation of the area also favours deposition on a slope connected to the Transantarctic Mountains in pre-Quaternary time, before carving of the Mackay sea valley (Hamilton et al., 1998).

Mass gravity flows are common in proglacial ice-proximal environments (Visser & Colliston, 1984, Powell & Molnia, 1989), but the deformed sediments in the lower part of the core are probably not of this type. Some of the folded sediments below 485 mbsf in CRP-2/2A have preserved lamination and bedforms, and are relatively rich in organic matter, suggesting that redeposition of more ice-distal facies occurred. Modioloid bivalves recovered from sediments below 441 mbsf (Taviani et al., this volume) are not compatible with ice grounded at sea level near the drill-site. Other paleoenvironmental data, including pollen (Askin & Raine, this volume), calcareous nannoplankton (Watkins & Villa, this volume), and clay mineralogy data (Ehrmann, this volume) show that climate for the interval below 444 mbsf was probably milder than for the interval above this level.

Relatively undisturbed bioturbated sandstones with relatively high marine productivity are present at 444-485 mbsf and at 545-570 mbsf, suggesting that the deformation was episodic and consisted of multiple events separated by relatively stable periods. The dominance of *Modiolus* sp. in the macrofossil assemblages in the lower part of the core suggests that the paleoenvironment was deprived of oxygen and enriched in hydrogen-sulphide. A distinct marine diagenetic assemblage of gypsum, pyrite and carbonate nodules is present below 445 mbsf (Cape Roberts Science Team, 1999), and only present in traces above this depth in the core, suggesting that early Oligocene mass-gravity flows took place in a deeper part of the shelf, below wave base.

COMPARISON TO OTHER CENOZOIC PALAEOENVIRONMENTAL RECORDS

Extensive mass-movement in an ice-distal environment characterises the early Oligocene section of CRP-2/2A. Gas hydrates may have formed periodically as suggested by the mosaic breccias below *ca.* 500 mbsf. Dissociation of gas hydrates may occur as a response to rapid sea level change and leads to sediment instability and slope failure (Paull et al., 1996; Maslin et al., 1998). Haq (1998) points out that $\delta^{13}C$ excursions at the Eocene-Oligocene boundary and in the mid-Oligocene could relate to gas hydrate response to sea level. Although the exact temporal relation between structures, $\delta^{13}C$ excursions and sea level remains ambiguous, the hypothesis of gas-hydrates as a cause of brecciation and slope failure in CRP-2/2A is testable if more chemical data become available.

A major unconformity in the CIROS-1 hole separates Eocene?-lower Oligocene strata from upper Oligocene-lower Miocene strata (Harwood et al., 1989; Wilson et al., 1998). In CRP-2/2A, the exact position of the mid-Oligocene unconformity is not yet established, but the interval in which it occurs is dominated by diamictites with a Transantarctic Mountains provenance (Cape Roberts Science Team, 1999). Macroscopic evidence of grounded ice occurs down to 364 mbsf within this interval (Fig. 8). Whether the grounded ice originated as alpine glaciers or an extensive ice-sheet cannot be established from the deformation record. However, the presence of a mid-Oligocene ice sheet in Antarctica is compatible with mid-Oligocene eustatic events (Fig. 8) and other stratigraphic records from the Antarctic continental margin. By early

Oligocene time the edge of the Lambert Glacier/Amery Ice Shelf complex in the Prydz Bay area was grounded 140 km beyond the edge of the present-day floating ice, suggesting that the East Antarctic ice sheet was fully developed by that time (Hambrey et al., 1989b).

The uppermost Oligocene sediments in CRP-2/2A lack macroscopic evidence of grounded ice (Fig. 8). Some upper Oligocene diamictites in CIROS-1 were related to grounded ice, although debate exists as to the position of the grounding events in the core (Hambrey et al., 1989a, Fielding et al., 1997, Hiemstra, 1999). Late Oligocene glacial sediments were also encountered in DSDP site 28 in the Central Ross Sea (Hayes & Frakes, 1975). Perhaps late Oligocene glaciation in the Ross Sea was characterised by small ice caps on exposed structural highs, as suggested by De Santis et al. (1997), and the rising Transantarctic Mountains may have prevented East-Antarctic ice from flowing onto the Ross Sea continental margin (Barrett, 1999). The Ross Sea provenance of upper Oligocene strata in CRP-2/2A is also in agreement with this interpretation.

Early Miocene strata from CRP-1, CRP-2/2A and CIROS-1 are brecciated, which could be related to glacial overriding. An oxygen-isotope record of the Oligocene-Miocene boundary (Zachos et al., 1997) shows that a late Oligocene through early Miocene warming trend was terminated by rapid cooling in the middle Miocene. However, the record also suggests that major changes in Antarctic ice-volume periodically interrupted the late Oligocene-early Miocene warming. In the Ross Sea, a middle Miocene shelf-wide unconformity marks the presence of grounded East- and West Antarctic ice on the shelf (Bartek et al., 1996). This unconformity is also present in the CRP-2/2A core: at 27 mbsf Pliocene-Quaternary strata directly overly early Miocene sediments (Cape Roberts Science Team, 1999). Early Miocene seismic stratigraphic sequences, which contain glacial seismic facies extend over large areas of the Ross Sea continental shelf, suggesting that continental glaciers may also have been draining onto the Ross Sea margin before the middle Miocene (Bartek et al., 1996). The sheared breccias in CRP-2/2A are in agreement with this interpretation.

CONCLUSIONS

The macroscopic and microscopic description of penecontemporaneous sediment deformation from CRP-2/2A contributes to the reconstruction of sedimentary environments in the Late Cenozoic record of the Ross Sea area:

1) The lower Oligocene section of the core is characterised as fjord-mouth delta sedimentation with periodic slumping, debris flows and grain-flows, based on the presence of contorted lamination, shear zones, inclined bedding, clastic dykes and microfaults. Gas-hydrates may have formed periodically, as is suggested by the presence of thin mosaic breccias.
2) The mid-Oligocene record marks the presence of grounded ice near the drill-site. Important sediment deformation features in this interval of core: clastic dykes, including a till wedge, microfaults, shear zones and a mudstone breccia. The presence of a grounded continental ice-sheet on the Ross Sea shelf is in agreement with other Antarctic stratigraphic records and a eustatic lowstand.
3) The upper part of the upper Oligocene succession was deposited in a stable depositional environment in the absence of grounded ice near the drillsite. Deformation is limited to a few clastic dykes and microfaults. The absence of grounded ice during most of the late Oligocene is in agreement with a general warming trend in the late Oligocene and early Miocene, as suggested by low-latitude proxy records.

The early Miocene section shows evidence of hydrofracturing of sediment and shearing related to grounded ice on the drillsite. The deformation may be related to short-lived episodes of glacial expansion during this generally warm climate interval with a relatively high sea level.

ACKNOWLEDGEMENTS

Many thanks go out to the drillers for providing such excellent core. Helpful comments from referees Juergen Ehlers and John Menzies greatly improved the manuscript. Peter Webb read earlier drafts and is thanked for discussions about gas-hydrates. Jaap van der Meer is thanked for editorial handling and discussions of some clastic dykes. He also provided the thin sections. Terry Wilson provided the core-scan images.

REFERENCES

Alley R.B., Cuffey K.M., Evenson E.B., Straaser J.C., Lawson D.E. & Larson G.J., 1997. How glaciers entrain and transport basal sediment: physical constraints. *Quaternary Science Reviews*, **16**, 1017-1038.

Baker J.C. & Fielding C.R., 1998. Diagenesis of glacimarine Miocene strata in CRP-1, Antarctica. *Terra Antartica*, **5**(3), 647-653.

Barrett P.J. & McKelvey B.C., 1986. Stratigraphy. In: Barrett, P.J. (ed.), Antarctic Cenozoic history from the MSSTS-1 drillhole, McMurdo Sound. *DSIR Bulletin*, **237**, 9-15.

Barrett P.J., 1999. Antarctic climate history over the last 100 Million years. In: Barrett, P.J. & Orombelli, G., (eds.). Proceedings of the Workshop: Geological Records of Global and Planetary Changes. *Terra Antartica Reports*, **3**, 53-72.

Bartek L.R., Henrys S.A., Anderson J.B. & Barrett P.J., 1996. Seismic stratigraphy of McMurdo Sound, Antarctica: implications for glacially influenced early Cenozoic eustatic change? *Marine Geology*, **130**, 79-98.

Bergman L., 1982. Clastic dykes in the Aland Islands, SW Finland and their origin. *Geological Survey of Finland Bulletin*, **317**, 33 pp.

Bohrmann G., Greinert J., Suess E. & Torres M., 1998. Authigenic carbonates from the Cascadia subduction zone and their relation to gas hydrate stability. *Geology*, **26**(7), 647-650.

Boulton G.S. & Caban P., 1995. Groundwater flow beneath ice sheets; Part II- Its impact on glacier tectonic structures and moraine formation. *Quaternary Science Reviews*, **14**, 563-587.

Boulton G.S. & Hindmarsh R.C.A., 1987. Sediment deformation beneath glaciers: rheology and geological consequences. *Journal of Geophysical Research*, **92**, **B9**, 9059-9082.

Brodzikowski K. & Van Loon A.J., 1985. Penecontemporaneous non-tectonic brecciation of unconsolidated silts and muds. *Sedimentary Geology*, **41**, 269-282.

Cape Roberts Science Team, 1998. Initial report on CRP-1, Cape Roberts Project, Antarctica. *Terra Antartica*, **5**(1), 187p.

Cape Roberts Science Team, 1999. Studies from the Cape Roberts Project, Ross Sea, Antarctica. Initial Report on CRP-2/2A. *Terra Antartica*, **6**(1/2), 173p.

Croot D.G., 1988. Morphological, structural and mechanical analysis of neoglacial ice-pushed ridges in Iceland. In: Croot, D.G. (ed.), *Glaciotectonics: Forms and Processes*. Balkema, Rotterdam, the Netherlands.

De Santis L., Brancolini G., Busetti M, & Marchetti A., 1997. Seismic sequences and Late Cenozoic glacial history in the Ross Sea. In: Ricci, C.A. (ed.), *The Antarctic Region: Geological Evolution and Processes*, Terra Antartica Publication, Siena, 781-790.

Dionne J.-C. & Shilts W.W., 1974. A Pleistocene clastic dike, Upper Chaudiere Valley, Quebec. *Canadian Journal of Earth Sciences*, **11**, 1594-1605.

Dreimanis A., 1993. Small to medium-sized glacitectonic structures in till and in its substratum and their comparison with mass movement structures. *Quaternary International*, **18**, 69-79.

Dreimanis A. & Rappol M., 1997. Late Wisconsinan sub-glacial clastic intrusive sheets along Lake Erie bluffs, at Bradtville, Ontario, Canada. *Sedimentary Geology*, **111**, 225-248.

Echelmeyer K. & Wang Z., 1987. Direct observations of basal sliding and deformation of basal drift at subfreezing temperatures. *Journal of Glaciology*, **33**(113), 83-98.

Fielding C.R., Woolfe K.J., Purdon R.G., Lavelle M. & Howe J.A., 1997. Sedimentological and stratigraphical re-evaluation of the CIROS-1 core, McMurdo Sound, Antarctica. *Terra Antartica*, **4**(2), 149-160.

Hambrey M.J., Barrett P.J. & Robinson P.H., 1989a. Stratigraphy. In: Barrett, P.J. (ed.), Antarctic Cenozoic history from the CIROS-1 drillhole, McMurdo Sound. *DSIR Bulletin*, **245**, 23-48.

Hambrey M.J., Larson B. & Ehrmann W. U., 1989b. Forty million years of Antarctic glacial history yielded by Leg 119 of the Ocean Drilling Program. *Polar Record*, **25**(153), 99-106.

Hamilton R.J., Sorlien C.C., Luyendyk B.P., Bartek L.R. & Henrys S.A., 1998. Tectonic regimes and structural trends off Cape Roberts, Antarctica. *Terra Antartica*, **5**(3), 261-272.

Hampton M.A., Lee H.J. & Locat J., 1996. Submarine landslides. *Reviews of Geophysics*, **34**(1), 33-59.

Haq B.U., Hardenbol J., & Vail P.R., 1987. Chronology of fluctuating sea level since the Triassic. *Science*, **235**, 1156-1167.

Haq B.U., 1998. Natural gas hydrates: searching for long-term climatic and slope-stability records. In: Henriet, J.-P. & Mienert, J. (eds.), Gas Hydrates: Relevance to World Margin Stability and Climate Change. *Geological Society London, Special Publ.* **137**, 303-318.

Harwood D.M., Barrett P.J., Edwards A.R., Rieck H.J. & Webb P.-N., 1989. Biostratigraphy and chronology. In: Barrett, P.J. (ed.), Antarctic Cenozoic history from the CIROS-1 drillhole, McMurdo Sound. *DSIR Bulletin*, **245**, 231-239.

Hayes D.E. & Frakes L.A., 1975. *Initial reports of the Deep Sea Drilling Project*. Washington, DC, US Government Printing Office, **28**, 1017 p.

Hiemstra J.F., 1999. Microscopic evidence of grounded ice in the sediments of the CIROS-1 core, McMurdo Sound, Antarctica. *Terra Antartica*, **6**(4), 365-376.

Kvenvolden K.A., 1993. Gas hydrates - geological perspective and global change. *Reviews of Geophysics*, **31**(2), 173-187.

Larsen E. & Mangerud J., 1992. Subglacially formed clastic dykes. *Sveriges Geologiska Undersöking*, **81**, 163-170.

Martinsen O., 1994. Mass movements. In: Maltman, A. (ed.), *The Geological Deformation of Sediments*. Chapman & Hall, London, U.K., p. 127-165.

Maslin M., Mikkelsen N., Vilela C. & Haq B.U., 1998. Sea-level- and gas-hydrate-controlled catastrophic sediment failures of the Amazon Fan. *Geology*, **26**(12), 1107-1110.

Murray T., 1997. Assessing the paradigm shift: deformable glacier beds, *Quaternary Science Reviews*, **16**, 995-1016.

Odonne F., Menard I., Massonnat G.J. & Rolando J.-P., 1999. Abnormal reverse faulting above a depleting reservoir. *Geology*, **27**(2), 111-114.

Passchier S., Wilson T.J. & Paulsen T.S., 1998. Origin of Breccias in the CRP-1 Core. *Terra Antartica*, **5**(3), 401-409.

Paull C.K., Buelow W.J., Ussler III W. & Borowski W.S., 1996. Increased continental margin slumping frequency during sea level lowstands above gas hydrate-bearing sediments. *Geology*, **24**(2), 143-146.

Powell R.D. & Molnia B. F., 1989. Glacimarine sedimentary processes, facies and morphology of the south-east Alaska shelf and fjords. *Marine Geology*, **85**, 359-390.

Rijsdijk K.F., Owen G., Warren W.P., McCarroll D., & Van der Meer J.J.M., 1999. Clastic dykes in over-consolidated tills: evidence for subglacial hydrofracturing at Killiney bay, eastern Ireland. *Sedimentary Geology* **129**, 111-126.

Shanmugam G., Bloch R.B., Mitchell S.M., Beamish G.W.J., Hodgkinson, R.J., Damuth J.E., Straume T., Syvertsen S.E. & Shields K.E., 1995. Basin-floor fans in the North Sea: sequence stratigraphic models vs. sedimentary facies. *AAPG Bulletin* **79**(4), 477-512.

Syvitski J.P.M., Burrell D.C. & Skei J.M., 1987. *Fjords, Processes and Products*. Springer Verlag, New York, U.S.A., 379 p.

Van der Meer J.J.M., Evenson E.B. & Rabassa J.O., 1994. Observations on the sedimentology of some clastic dykes from glacial environments. *Abstract IGCP Symposium "The termination of the Pleistocene in South America"*, Tierra de Fuego, Argentina, March 15-25, 1994.

Van der Wateren F.M., 1995. Structural geology and sedimentology of push moraines. Processes of soft sediment deformation in a glacial environment and the distribution of glaciotectonic styles. *Mededelingen van de Rijks Geologische Dienst*, **54**, Haarlem, The Netherlands, 168p.

Visser J.N.J. & Colliston W.P., 1984. The origin of soft-sediment deformation structures in Permo-carboniferous glacial and proglacial beds, South Africa. *Journal of Sedimentary Petrology*, **54**(4), 1183-1196.

Von Brunn V. & Talbot C.J., 1986. Formation and deformation of subglacial intrusive clastic sheets in the Dwyka formation of northern Natal, South Africa. *Journal of Sedimentary Petrology*, **56**(1), 35-44.

Wilson G.S., Roberts A.P., Verosub K.L., Florindo F., & Sagnotti L., 1998. Magnetobiostratigraphic chronology of the Eocene-Oligocene transition in the CIROS-1 core, Victoria Land margin, Antarctica: Implications for Antarctic glacial history. *GSA Bulletin*, **110**(1), 35-47.

Winslow M.A., 1983. Clastic dike swarms and the structural evolution of the foreland fold and thrust belt of the southern Andes. *GSA Bulletin*, **94**, 1073-1080.

Zachos J.C., Flower B.P. & Paul H., 1997. Orbitally paced climate oscillations across the Oligocene-Miocene boundary. *Nature*, **388**, 567-570.